ADVANCED FUNCTIONAL MATERIALS
www.afm-journal.de

Elastic Modulus Dependence on the Specific Adhesion of Hydrogels

*Hanqing Wang, Fawad Jacobi, Johannes Waschke, Laura Hartmann, Hartmut Löwen, and Stephan Schmidt**

Mechanosensitivity in biology, e.g., cells responding to material stiffness, is important for the design of synthetic biomaterials. It is caused by protein receptors able to undergo conformational changes depending on mechanical stress during adhesion processes. Here the elastic modulus dependence of adhesive interactions is systematically quantified using ligand–receptor model systems that are generally not thought to be mechanosensitive: biotin–avidin, mannose–concanavalin A, and electrostatic interactions between carboxylic acids and polycationic surfaces. Interactions are measured by microgel sensors of different stiffness adhering to surfaces presenting a corresponding binding partner. Adhesion is generally decreased for softer microgels due to reduced density of binding partners. Density-normalized data show that low-affinity carbohydrate ligands exhibit reduced binding in softer networks, probably due to increased network conformational entropy. However, in case of stronger interactions with large interaction range (electrostatic) and large lifetime (biotin–avidin) density normalized adhesion is increased. This suggests compensation of entropic repulsion for softer networks probably due to their increased mechanical deformation upon microgel adhesion and enhanced cooperative binding. In essence, experiments indicate that soft interacting polymer materials exhibit entropic repulsion, which can be overcome by strongly interacting species in the network harnessing network flexibility in order to increase adhesion.

1. Introduction

Important cell processes including development, communication, and inflammation are mediated by the adhesive interactions of biological interfaces such as the glycocalyx or the extracellular matrix.[1] These adhesive interactions are controlled by the dynamic binding and unbinding of various biomolecules, e.g., carbohydrates, proteins, or lipids. Additionally, physical and chemical properties of the interface and surrounding materials influence the specific adhesion of biointerfaces. For example, the stiffness of a cell substratum has a direct effect on cellular adhesion, spreading, and development of the cell.[2] In order to explain these phenomena, various cell adhesion receptors have been identified and shown to respond to cytoskeletal stresses, thereby adapting to the mechanical properties of the matrix.[3] The premiere example in this regard are integrin receptors forming adhesion complexes with peptide ligands. The prevalent theories hold that integrin mechanosensitivity and cell response to matrix stiffness is due to molecular sensing via protein conformational changes upon mechanical stress followed by signal transduction.[4] Although not broadly recognized, theoretical work showed that it could be the ligand–protein receptor interaction itself that is sensitive to the mechanical and structural properties of the involved material surfaces. This has been shown by modeling of ligand presenting flexible lipid membranes[5,6] or by simulating the impact of extracellular matrix stiffness on integrin adhesion.[7] These studies take into account that cell adhesion ligands are attached to flexible surfaces that are spatially dynamic due to thermal fluctuations or by mechanical forces imposed by the cell.

Following this argument, specific adhesion could be intrinsically mechanosensitive, in particular for mechanically flexible materials such as the cells glycocalyx. The glycocalyx is a gel-like carbohydrate layer surrounding all eukaryotic cells. It presents carbohydrate ligands that dominate in many binding processes, including adhesion and recognition.[8] The carbohydrate ligands can be thought to be attached to a highly swollen, flexible polymeric network that can stretch and bend in order to interact. As suggested by simulations on single polymer chains,[9,10] the specific interactions of such a material could be directly affected by its stiffness. This is because the stiffness of a polymer network is related to its mesh size, and in turn, the mesh size may control specific interactions due to several factors. For example, the loss in conformational freedom (entropy) of the network upon binding, the spatial range of the ligands to "look" for a binding partner, or the bending rigidity of the network that has to be overcome in order to form adhesion sites.

Dr. H. Wang, F. Jacobi, Prof. L. Hartmann, Prof. S. Schmidt
Institute for Organic and Macromolecular Chemistry
Heinrich-Heine-Universität
Universitätsstrasse 1, 40225 Düsseldorf, Germany
E-mail: stephan.schmidt@hhu.de
J. Waschke
Max Planck Institute for Human Cognitive and Brain Sciences
Stephanstraße 1a, 04103 Leipzig, Germany
Prof. H. Löwen
Theoretical Physics II: Soft Matter
Heinrich-Heine-Universität
Universitätsstrasse 1, 40225 Düsseldorf, Germany

DOI: 10.1002/adfm.201702040

In addition, theoretical work showed that multivalent and cooperative binding depends on the molecular flexibility of the interacting binding partners.[7,11] Therefore material stiffness may affect multivalent binding modes in case of soft, hydrogel-like materials with multivalent presentation of ligands.

In essence, several theoretical studies showed that ligand–receptor mediated adhesion of soft polymeric surfaces is affected by the mechanical flexibility of the involved materials. This could in part explain the mechanosensitive nature of various processes on the cell level, including adhesion. In order to verify up to what extent mechanical properties affect adhesion and related biological processes, more experimental data are needed. Therefore, here we aim at directly measuring the effect of material stiffness on specific adhesion using ligand functionalized hydrogel particles, so-called soft colloidal probes (SCPs), as a simplified model system for soft biological materials like the glycocalyx. The working principle of adhesion measurements with the SCPs is outlined in **Figure 1**. Briefly, the SCPs undergo mechanical deformation when adhering to a material surface[12,13] and the mechanical deformation can be readily read out by an interferometric technique (reflection interference contrast microscopy, RICM)[14] and then related to the adhesion energy of the SCP resting on a surface using a model developed by Johnson, Kendall, and Roberts (JKR model)[15]

$$W_{\mathrm{adh}} = \frac{E_{\mathrm{eff}} a^3}{6\pi R^2} \tag{1}$$

where a is the radius of contact, R radius of the SCP, and $E_{\mathrm{eff}} = [4E/3(1 - \nu^2)]$ its effective elastic modulus, with ν the Poisson ratio and E the elastic modulus of the SCP. One important advantage of this method is that hydrogel particles directly act as adhesion sensors and their elastic modulus can be easily adjusted from 10 to 500 kPa. In addition, due to their water-swollen poly(ethylene glycol) (PEG) matrix and the ability to functionalize the matrix with various biomolecules, e.g., proteins,[16] peptides,[17] or carbohydrates,[18] SCPs show biomimetic properties and reflect adhesion close to the biological context. Due to their biomimetic properties, SCPs have recently been used as probes for atomic force microscopy (AFM) based adhesion measurements cells[19] and biomaterial surfaces.[20,21]

Here, SCPs of varying crosslinking density and elastic moduli will be used to systematically study the effect of material stiffness on specific adhesion. We study three different types of specific interactions: electrostatic interactions using carboxylic acid functionalized SCP adhering on polycationic surfaces, strong ligand–receptor interactions between biotin and avidin, and weak carbohydrate interactions between mannose and Con A. We expect that the elastic modulus dependence of these interactions will differ and allow us to gain a deeper understanding on mechanosensitivity based on biomolecular interactions of soft networks. By varying the interacting molecules in the PEG-network, we can additionally analyze the effect of interaction range, ligand–receptor affinity, and complex life time on adhesion. We discuss the results with respect to entropy contribution when adhering polymer networks of different elastic moduli and also consider possible cooperativity effects that may occur when adhering material surfaces presenting multiple binding partners.

2. Results

2.1. Synthesis of SCPs with Different Elastic Moduli and Ligand Functionalization

As outlined in **Figure 2** we prepared SCPs with a soft hydrogel matrix by crosslinking poly(ethylene glycol) (8 kDa) diacrylamide (PEG_{8kDa}–dAAm) macromonomers in an aqueous dispersion.[12] In order to control the elastic modulus, different amounts of crotonic acid (CA) were added before polymerizing the macromonomers. CA adds to the radicals at growing PEG–dAAm chains and essentially caps the crosslinking sites, as it is known to not homopolymerize under the applied conditions. Therefore, increasing amounts of CA will lead to gradually softer SCPs due to reduced crosslinking. The elastic moduli of the final SCPs were determined by AFM force-indentation measurements (Section S1, Supporting Information). The

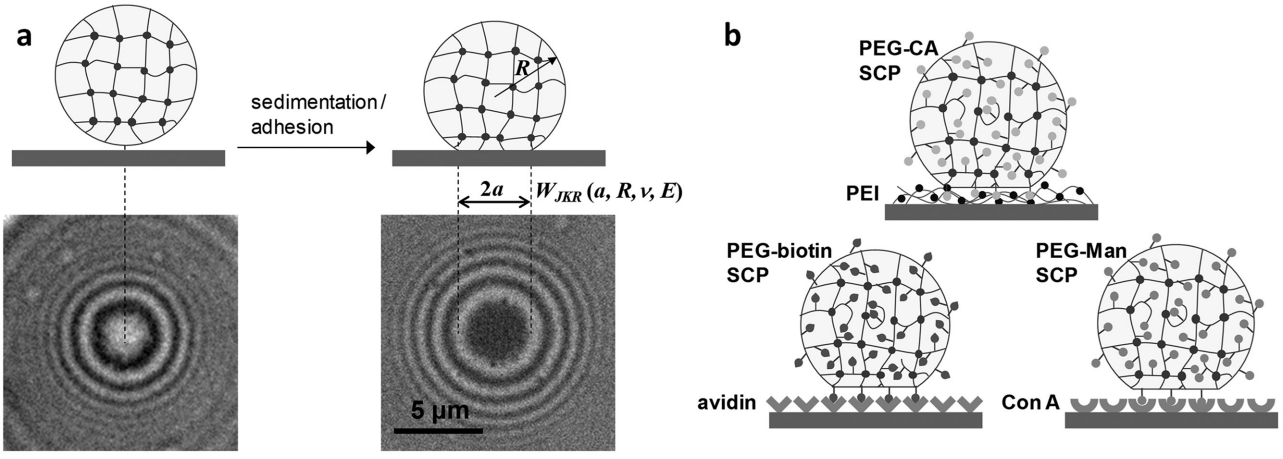

Figure 1. a) Principle of the JKR adhesion measurements with soft SCPs and typical RICM images (bottom) right before and after adhesion. The dark area in the middle signifies the SCP contact area with the glass slides. b) Overview of the adhesion assays with various SCPs functionalization on glass slides with the appropriate binding partner.

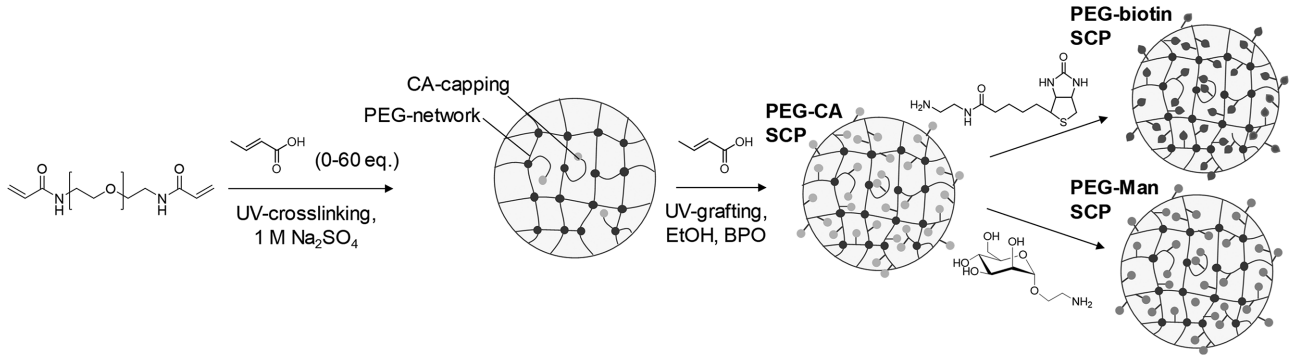

Figure 2. Overview of the synthetic approach toward crotonic acid (CA) and ligand functionalized PEG SCPs.

force-indentation data were evaluated with an appropriate model taking into account that the SCPs deform at the indenter site and the contact site with the solid substrate.[22]

As a means to overall increase and equalize the density of CA groups regardless of SCP crosslinking density, more CA groups were grafted in the PEG–dAAm network using benzophenone as active photophore.[23,24] As a result, we obtained PEG–CA SCPs with a CA functionalization degree on the order of 120 μmol g^{-1} (dried particles) as measured via toluidine blue titration (Section S3, Supporting Information). The PEG–CA SCPs have a polyanionic character due to the negative charges of deprotonated crotonic acid and were thus directly employed in electrostatic adhesion measurements on cationic poly(ethylene imine) (PEI) coatings. For the preparation of ligand functionalized systems, PEG–CA SCPs were further functionalized by activating the carboxylic acids with benzotriazol-1-yl-oxytripyrrolidinophosphonium hexafluorophosphonate/hydroxybenzotriazole (PyBOP/HOBt) followed by amide formation with aminoethyl-linked mannose and aminoethyl-linked biotin. The degree of functionalization was determined by a second titration step with toluidine blue that essentially quantified the reduction of carboxylic acids due to amidation upon ligand coupling. The conversion was on the order of 90%, i.e., functionalization degrees on the order of 100 μmol g^{-1} were achieved. Considering the molecular weight of PEG–dAAm macromonomers of 8000 kDa, this means that roughly 0.8 ligand molecules per macromonomer were coupled to the network.

It is important to note that in dry state the density of CA groups and ligand molecules is rather invariant with respect to the crosslinking degree. However, there were significant differences in functional group density when the SCPs were swollen in aqueous solution. This is simply because softer SCPs with a lower crosslinking degree swell more in good solvents such as water, thereby showing a stronger reduction in functional group concentration as compared to stiffer SCPs. This can be directly seen from microscopic images of toluidine blue stained PEG–CA SCPs in water (Section S2, Supporting Information). Softer SCPs show a strongly reduced staining, signifying lower concentration of CA in the PEG network. In order to quantify the functional group densities in the swollen state, we have measured the degree of swelling of PEG–CA SCPs as a function of their elastic modulus. This was done by measuring the size of individual SCPs by optical microscopy in solution (swollen state) and by AFM in dry state (Section S2, Supporting Information). Although the experimental error was rather large, we found that for PEG–CA SCPs the scaling of elastic modulus and degree of swelling were in good agreement with experiments on macroscopic PEG gels by Hild et al.[25] Therefore, we used their empirical scaling laws for calculating the SCP swelling degree and functional group concentration in the PEG network.

2.2. Electrostatically Driven Adhesion of PEG Hydrogels

After the introduction of anionic CA groups in the PEG network, we set out to measure the electrostatically driven adhesion of PEG–CA SCPs with varying elastic modulus on cationic PEI films on a glass slide. It can be estimated that the density of anionic CA groups in the network was five orders of magnitude smaller as compared to the density of cationic groups in the PEI layer (≈100 μmol L^{-1} vs ≈10 mol L^{-1} considering the branched PEI molecules are completely stretched). In a typical adhesion measurement, the SCPs were dispersed in the measurement media and then a droplet of the dispersion was added to the PEI slides mounted in a liquid cell containing the measurement media. Then, SCPs gently sedimented on the glass slide and adhesion took place. Since the SCPs were soft, adhesion led to mechanical deformation of the PEG network and to formation of a micrometer-sized contact area with the glass slide. The contact radius as well as the particle radius can be quantified by means of RICM (Section S4, Supporting Information) and with the previously determined elastic modulus of the SCPs, the JKR adhesion energy can be calculated (Equation (1)).

The measurements were conducted at varying sodium chloride concentration (1×10^{-6} M–150×10^{-3} M) to show the effect of electrostatic screening on the interaction between PEG–CA SCPs and the PEI surface. As expected, the contact radius significantly decreases when increasing the sodium chloride concentration, as seen in the RICM images (**Figure 3**b) and the contact radius versus SCP radius plots (Figure 3a).

This demonstrates that adhesion was overall driven by electrostatic interactions. We found that W_{adh} increased with elastic modulus regardless of the sodium chloride concentration (**Figure 4**a; Section S4, Supporting Information). The main reason for this is the increased concentration of charged CA groups in stiffer, more crosslinked SCPs. As discussed above, this is due

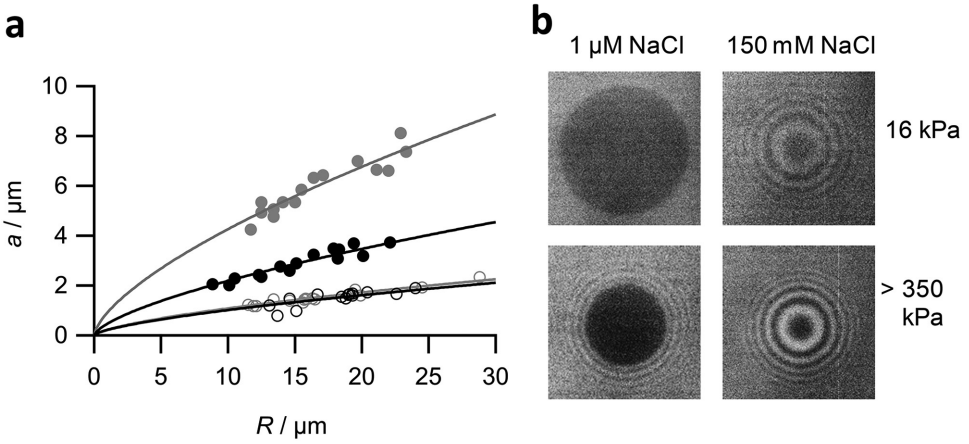

Figure 3. PEG–CA SCPs adhering on PEI surfaces. a) Contact radius a versus SCP radius R in 1×10^{-6} M NaCl of softest (grey) and stiffest (black) SCPs (full symbols) and in 150×10^{-3} M sodium chloride (empty symbols). b) Typical RICM images of the softest (top) and stiffest (bottom) SCPs in 1×10^{-6} M NaCl (left) and 150×10^{-3} M sodium chloride (right).

to reduced swelling of the stiffer SCPs resulting in increased density of CA groups in the PEG network. As can be seen from the scaling exponents of E in Figure 4, the elastic modulus dependence of W_{adh} was increased for larger sodium chloride concentration. Adhesion data for intermediate salt concentrations confirm this trend (Section S4, Supporting Information). By normalizing adhesion data with respect to CA concentration, $W_{adh}^{norm} = W_{adh}/[CA]$, we can depict the adhesive potential of CA groups in the PEG network as a function of elastic modulus (Figure 4b). For the sake of comparability, we present the normalized adhesion as the relative change in normalized adhesion energy using the maximum value: $W_{adh}^{norm}/W_{max.adh}^{norm}$. Interestingly, the elastic modulus dependence of the adhesive potential was different depending on the sodium chloride concentration. In case of 150×10^{-3} M sodium chloride the normalized adhesion energies increased by a factor of five from the softest to the stiffest SCPs. At low sodium chloride concentration of 1×10^{-6} M, the normalized adhesion energy decreased by a factor of two for the stiffest SCPs compared to the softest ones.

In addition, we found that the measured relation between elastic modulus E and crotonic acid concentration [CA] was consistent with theoretical predictions. For a network consisting of entropically elastic polymer chains, E can be related to the polymer segment density $C_p \approx E^{4/9}$.[26] Since the density of grafted CA molecules in the PEG network is proportional to C_p, the measured relation between E and [CA] agreed well with the predicted $E^{4/9}$ scaling (Figure 4a).

2.3. Hydrogel Adhesion Mediated by Weak and Strong Ligand–Receptor Interactions

In the following, we studied ligand/receptor mediated adhesion as a function of elastic modulus and affinity of the binding partners. As strong and weak affinity ligands in the PEG network, we synthesized biotin (PEG–biotin) and mannose (PEG–Man) functionalized SCPs, respectively, as explained in the preparation section above. Consequently, the adhesion studies were carried out on biotin and mannose binding receptor surfaces, i.e., glass slides functionalized with avidin and Con A, respectively. The glass surfaces were first modified by an epoxy-containing silane layer that covalently

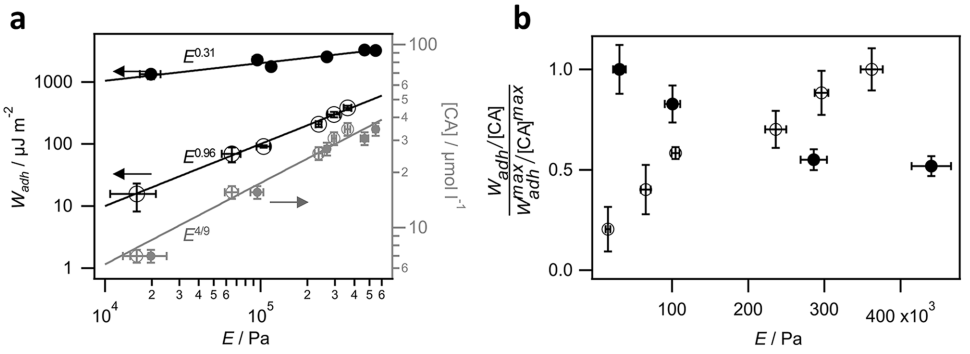

Figure 4. PEG–CA SCPs on PEI surfaces in 1×10^{-6} M sodium chloride (full symbols) and in presence of 150×10^{-3} M sodium chloride (empty symbols). a) The log–log plot of W_{adh} (left axis, black symbols) and CA concentration (right axis, gray symbols) as a function of elastic modulus. Power law fits (solid black lines) give $W_{adh} \approx E^{0.31}$ (water) and $W_{adh} \approx E^{0.96}$ (150×10^{-3} M sodium chloride). The solid red line denotes the theoretical scaling law[26] $[CA] \approx E^{4/9}$. b) Concentration-normalized adhesion values as function of elastic modulus. Note the monotonic increase and decrease of the adhesive potential versus E in presence and absence of salt, respectively ($n > 20$, error bars represent standard deviations).

binds the protein receptors. As suggested by amino acid analysis in preceding studies,[20] this treatment leads to densely packed protein surfaces. After rinsing and equilibrating the surfaces in the measurement buffers, the corresponding SCPs were added and W_{adh} was measured using the JKR approach (**Figure 5**).

Again, owing to the reduced ligand densities of softer networks, the overall adhesion energies increased with elastic modulus, as expected. Over the whole range of elastic moduli we saw that W_{adh} was larger for biotin/avidin complexes as compared to mannose/Con A complexes (**Figure 6**a). This could be expected given the higher binding affinity of the biotin–avidin pair (35 k_BT)[27] compared to the mannose–Con A pair (7.5 k_BT).[28] Note that the elastic modulus dependence of W_{adh} was much steeper in case of mannose–Con A as compared to biotin–avidin ($W_{adh} \approx E^{0.98}$ and $W_{adh} \approx E^{0.44}$). This trend is confirmed when plotting the adhesive potential of the ligands, i.e., adhesion data normalized with the ligand concentration $W_{adh}^{norm} = W_{adh}/[\text{ligand}]$ (Figure 6b), where [ligand] denotes the concentration of mannose or biotin in the PEG network. For biotin–avidin the adhesive potential of the ligands remained constant for a large range of elastic moduli and was slightly decreasing in the high elastic modulus range. Mannose–Con A, on the other hand, showed a strong increase in adhesion in the lower elastic modulus range (16–100 kPa). Overall, we observed a marked difference in the elastic modulus dependence of W_{adh} for the low- and high-affinity binding partners. The low-affinity mannose/Con A pair binds stronger on stiffer PEG networks, whereas the high-affinity pair biotin/avidin shows a small reduction in adhesive potential in this case.

3. Discussion

The present study provides clear evidence that the network elastic modulus affects the specific adhesion of ligand molecules as well as electrostatically driven adhesion. The elastic modulus dependence of SCP adhesion was not merely due to variation of binding partner density (polymer segment density scaling scales with $E^{4/9}$). This can be seen from density normalized adhesion data in Figures 4b and 6b. Additionally, comparison with previous adhesion measurements on SCPs with varying ligand density but constant elastic modulus[23] shows that the elastic modulus effect on adhesion is significantly stronger than the ligand density effect originating from the $E^{4/9}$ scaling (Section S6, Supporting Information).

More importantly, the adhesion energy–elastic modulus behavior depends significantly on the overall strength of the interaction. The weak binding systems PEG–CA at elevated electrolyte concentration and PEG–Man show a strong decrease of the adhesive potential with decreasing elastic modulus, whereas the strong binding SCPs, PEG–CA in water and PEG–biotin, show the opposite trend (Figures 4b and 6b). For the discussion of these trends, different effects such as the entropic costs of adhering flexible polymer networks, cooperative binding at the surface, as well as mechanical deformation upon adhesion will be considered.

First, we look at the overall reduction in adhesion at smaller elastic modulus as observed for the weak binding PEG–CA gels at high sodium chloride concentration on PEI surfaces and PEG–Man gels on Con A surfaces. We attribute this finding to the fact that polymer hydrogels are generally quite flexible and the energetic cost of entropically favored random polymer coils is large enough that reduction of conformational states upon polymer chain contact with the surface also reduces the overall adhesion. Accordingly, the entropic costs of adhering a softer network with more flexible polymer chains with more conformational states would be increased. In order to estimate the contribution of chain entropy to the elastic modulus dependence of adhesion, we propose a simple scaling theory describing the trends in our data. This theory incorporates the mesh size ξ of the crosslinked SCP and the typical spacing b between the two neighboring receptor–ligand binding sites explicitly and therefore goes beyond macroscopic elasticity theory. In our scaling theory, we do not consider any numerical prefactors. First of all, the adhesion energy is proportional to the bond energy U and ligand surface density $1/b^2$

$$W_{adh} \sim -U/b^2 \quad (2)$$

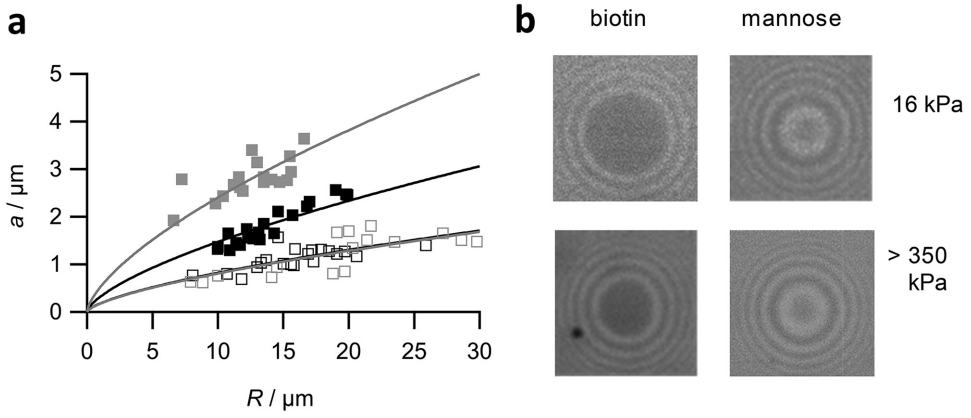

Figure 5. PEG–biotin (full symbols) and PEG–Man (open symbols) SCPs adhering to receptor surfaces. a) Contact radius a versus SCP radius R of softest (grey) and stiffest (black) SCPs. b) Typical RICM images of the softest (top) and stiffest (bottom) PEG–biotin SCPs (left) and PEG–Man SCPs (right).

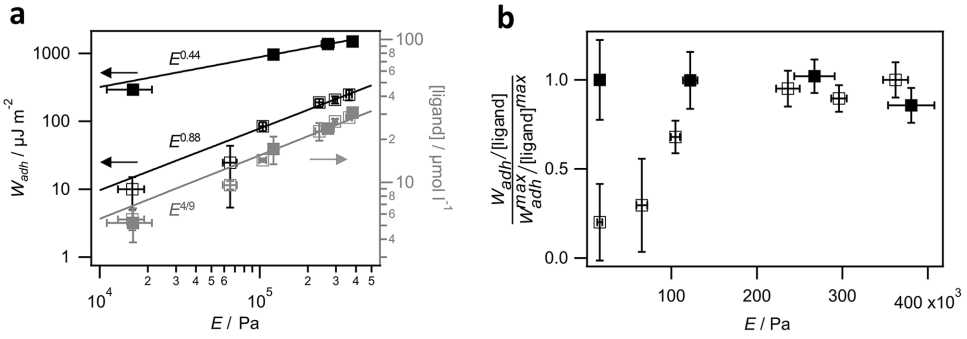

Figure 6. Adhesion energies of PEG–biotin (full symbols) and PEG–Man (open symbols) SCPs on receptor surfaces. a) The log–log plot of W_{adh} (left axis, black symbols) and ligand concentration (right axis, colored symbols) as a function of E. Power law fits (solid black lines) give $W_{adh} \approx E^{0.43}$ (PEG–biotin) and $W_{adh} \approx E^{0.88}$ (PEG–Man). The solid blue line denotes the theoretical scaling law [ligand] $\approx E^{4/9}$. b)The concentration-normalized adhesion values as function of elastic modulus. The adhesive potential of biotin ligand stays constant, while adhesion for mannose ligands increases with E ($n > 20$, error bars represent standard deviations).

The mechanical properties of polymer networks can be described by entropic elasticity, where E scales as

$$E \sim -kT/\xi^3 \tag{3}$$

Since $1/\xi^3$ is proportional to the crosslinker concentration, both crosslinking sites and ligand–receptor complexes at the surface imply two entropy costs relative to the free unlinked polymer. For our swollen polymer networks of varying crosslinking density, we can assume a simple proportionality between ligand spacing and mesh size, $b \approx \xi$. This scaling would reduce the overall entropy penalty since crosslinking and entropy costs upon surface binding coincide and therefore do only occur once. With this scaling argument and combining Equations (2) and (3) the adhesion energy scales as

$$W_{adh} \sim -U\left(E/kT\right)^{2/3} \tag{4}$$

The experimentally found scaling exponents $E^{0.88}$ (PEG–CA at 150×10^{-3} M NaCl) and $E^{0.96}$ (PEG–Man) are larger as compared to the predicted exponent $W_{adh} \approx E^{2/3}$ (Figures 4a and 6a). This deviation could be explained by experimental error, e.g., by only considering the measured bulk elastic modulus we neglect that dangling chains of soft networks are preferentially situated at the surface of the SCPs. In addition, the density of binding partners was assumed to be $1/b^2$. This may change due to the mechanical network deformation upon adhesion, which would be dependent on E, and therefore potentially change the scaling exponent. However, there is no straightforward theoretical approach to these problems. Nevertheless, entropy effects could explain the overall reduction in adhesive potential for increasing E in case of PEG–Man and PEG–CA in presence of salt (Figures 4b and 6b).

In case of the stronger binding SCPs, PEG–biotin and PEG–CA, at low salt concentration in the micromolar range we observed the opposite trend. The scaling exponents were significantly smaller ($E^{0.31}$ and $E^{0.44}$, respectively), as compared to the $E^{2/3}$ prediction. This means higher entropic costs for adhering softer networks were potentially compensated. In case of PEG–CA at low concentrations of NaCl, the PEI surface and the SCPs exhibit long-range attractive electrostatic interaction. For the micromolar sodium chloride concentration range tested (Section S4, Supporting Information) the Debye length is on the order of 0.1 μm. It could be argued that softer SCPs show larger vertical deformation when adhering, thereby being able to bring more charged CA groups closer to the cationic PEI layer (**Figure 7**). This leads to a positive feedback where the softer the network undergoes larger mechanical deformation, which in turn increases adhesion, thus further increasing mechanical deformation. According to the JKR theory, the adhesion induced deformation is due to the adhesive force $F_{adh} = 3\pi R W_{adh}$. Following Hertzian contact mechanics, the local compression near the contact area due to F_{adh} leads to deformation of the whole SCP which then approaches to the surface by a distance δ given by

$$\delta = \left(\frac{3F_{adh}\left(1-\nu^2\right)}{4ER^{1/2}}\right)^{2/3} \tag{5}$$

With this equation, it can be estimated that for the softest SCPs the vertical deformation is on the order of 1 μm. For the stiffest SCPs, the vertical deformation was only 200 nm. Therefore, softer SCPs vertically deformed more and were able to increase the electrostatic interaction by bringing internal anionic CA groups closer to the cationic surface. In presence of

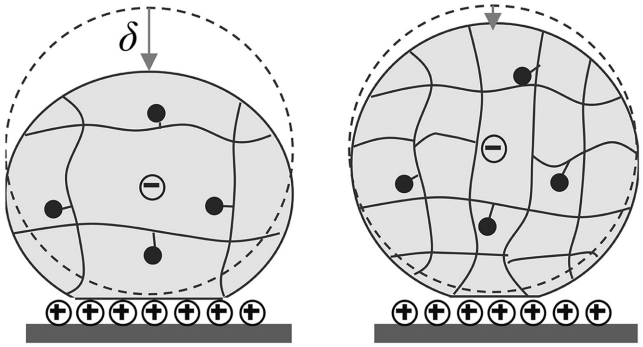

Figure 7. Vertical deformation upon adhesion of a soft SCP (left) is larger as compared to hard SCP (right) thus bringing anionic groups closer to the cationic surface.

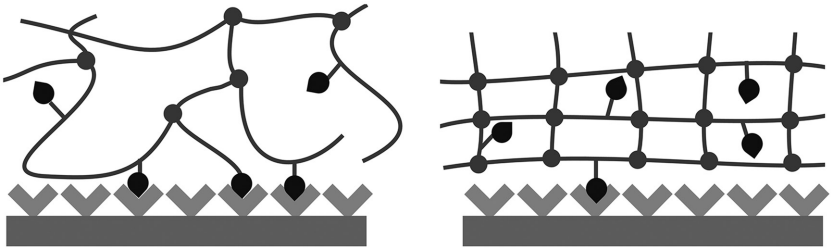

Figure 8. Higher spatial sampling range for receptor binding sites and cooperative binding enhance the adhesive potential of biotin ligands in case of soft networks (left). For stiff networks the spatial sampling range and cooperative binding are reduced.

salt, however, the $W_{adh} - E$ dependence is dominated by the entropic effect. This is due to the drastically reduced Debye length of about 1 nm in 150×10^{-3} M sodium chloride and the resulting screening of CA molecules that are not in direct contact with the PEI layer. Therefore, mechanical deformation of the SCP upon adhesion does not lead to significantly enhanced interaction with the PEI surface in case of high electrolyte concentrations.

The nonionic ligand/receptor interactions of PEG–Man and PEG–biotin SCPs have a short interaction range. Therefore, their different $W_{adh} - E$ scaling cannot be explained by binding range differences, but by the different lifetimes of the involved ligand–receptor complexes. The half-life of the mannose–Con A complex is on the order of a few seconds,[29] whereas biotin–avidin complexes last for several days.[30] The extremely slow unbinding rates of biotin–avidin may give rise to cooperative binding at the surface of the polymer network: Once a long-living complex has been formed, neighboring biotin ligands could be drawn closer to the receptor surface, thereby increasing their probability to also bind to the receptors (**Figure 8**). Such a mechanical coupling induces cooperative binding and is potentially stronger for softer networks due to their enhanced mechanical flexibility.[6,7] Another factor that may increase adhesion of softer networks in case of biotin is the large free energy of complex formation of 35 k_BT. This would enable binding of rather long, entropically costly polymer chains that have a large reach to effectively "probe" the avidin surface for binding sites. Adhesion measurements with the surface force apparatus and simulations have shown that biotin connected to long PEG-tethers showed enhanced binding for the entropically rare extended conformations.[6,10] However, binding of such long chains in case of low affinity Man ligands (7.5 k_BT) is less likely due to entropy costs. Therefore, softer SCPs with more long dangling chains show reduced adhesion in case of weak sugar based interactions, whereas strong biotin–avidin interactions (35 k_BT) can still contribute to adhesion.

It is generally believed that carbohydrate recognition of materials like the cells glycocalyx is due to multivalent and cooperative binding.[8] However, we observed an overall reduction in carbohydrate interaction with reduced SCP elastic modulus, which suggests the absence of cooperative binding between PEG–Man SCPs and Con A surfaces. On the other hand, here the density of carbohydrate ligands in the Man-SCP was orders of magnitudes smaller as compared to the natural glycocalyx, hence reduced multivalent binding and absence of cooperativity could be expected. To some extent the SCPs represent only a crude model system for natural biointerfaces. Nevertheless, the results show that for soft gel-like materials such as the cells glycocalyx, entropic repulsion acts against ligand recognition and needs to be taken into consideration when evaluating ligand–receptor mediated processes.

4. Conclusion

In summary, our work shows that for polymeric networks specific adhesion can be significantly affected by network elastic modulus. For weakly interacting networks, as seen for electrostatic adhesion in case of high electrolyte concentration or for low affinity sugar ligands adhering to Con A surfaces, adhesion was reduced at lower elastic modulus due to increased entropic repulsion of the network. For strongly interacting networks, like electrostatically adhering systems at low electrolyte concentration or for high affinity biotin ligands binding to avidin surfaces, adhesion was slightly increased for softer networks. This could be due to mechanical coupling inducing cooperative binding and large network deformation upon adhesion. Both effects potentially lead to a positive feedback compensating higher entropic costs of adhering softer polymer networks and enhance the overall adhesion. Therefore, this first quantitative study on elastic modulus effects and adhesion suggests that multivalency and cooperative binding required for many biological functions might be mediated by material stiffness directly. The SCP adhesion assay could help to gain insights into biological problems related to soft interface interactions and may also help to understand the design and function of new synthetic ligands in soft biomimetic materials. For example, entropic repulsion could be directly confirmed by measuring specific adhesion as a function of temperature. At this stage, the found relation between network stiffness on adhesion and the effect of interaction strength might be relevant for future biomaterial development, in particular for materials that are supposed to mimic soft scaffolds with cooperatively interacting ligands such as the cells glycocalyx.

5. Experimental Section

Materials: PyBOP was obtained from Carbolution Chemicals GmbH. Benzophenone and avidin were obtained from Thermo Fisher Scientific, N,N-Diisopropylethylamine (DIPEA) was obtained from Carl Roth. Con A was obtained from Cayman Chemicals. All other chemicals were obtained from Sigma-Aldrich. All water used here was produced by purification system (Barnstead MicroPure Thermo Scientific, Germany) with a resistivity higher than 18.2 MΩ cm at 25 °C.

Synthesis of Aminoethyl Linked Mannose and Biotin Ligands: Synthesis of an azido sugar derivative (2-azidoethyl) 2,3,4,6-tetra-O-acetyl-α-D-mannopyranoside was prepared according to a literature protocol.[31] Briefly, the general procedure for the amino sugar derivative starting from the azido sugar was performed as follows:[18] Under Ar atmosphere, to a solution of the azido sugar (1.5 g, 6.73 mmol) in tetrahydrofurane (THF) (100 mL), and $CHCl_3$ (4.0 mL), a catalytic amount of 10% palladium on carbon (10% w/w) was added. The mixture was stirred overnight at room temperature under a hydrogen atmosphere. Then, water (100.0 mL)

was added to redissolve precipitated material and the reaction mixture was filtered over Celite. The filtrate was concentrated removing the organic solvents and the resulting solution was washed with chloroform (3 × 50.0 mL). Lyophilization gave the HCl salt in quantitative yield. The synthesis of a biotin derivative for SCP functionalization was prepared according to Tao et al.[32]

Soft Colloidal Probe Preparation: PEG SCPs were synthesized by crosslinking a dispersion of PEG–dAAm macromonomer droplets in a similar manner as described previously.[12] PEG–dAAm (M_n 8000 Da) (50 mg, 6.3 µmol) was dispersed in a 1 M sodium sulfate/PBS (phosphate buffered saline) solution (10 mL). Varying amounts of crotonic acid (0–756 µmol) were added to change the elastic modulus of the microparticles. Then the UV photoinitiator Irgacure 2959 (1 mg, 4.5 µmol) was added to the dispersion and vigorously shaken and photopolymerized under UV light. The PEG SCPs were washed with water and stored in water. The resulting particles were 10–70 µm in diameter. Next, the PEG SCPs were grafted with CA to increase the number of functional groups.[23] Briefly, water was exchanged by ethanol, and benzophenone (250 mg, 1.4 mmol) and crotonic acid (1.5 g, 17.4 mmol) were added. Then the mixture was flushed with nitrogen for 30 s and irradiated with UV light for 900 s. The PEG–CA SCPs were washed with ethanol. In order to prepare ligand functionalized SCPs, PEG–CA SCPs dispersion (5 mL) was transferred in DMF (dimethylformamide) (5 mL) by repetitive centrifugation and washing/solvent exchange steps. According to the molar amount of carboxylic groups, PyBOP (10 eq.), HOBt (5 eq.), and DIPEA (10 eq.) were added to the PEG–CA SCP dispersion and shaken for 10 min to activate the carboxylic groups. Then, aminoethyl linked mannose or biotin (10 eq.) was added to the dispersion and shaken for 3 h, then washed with DMF. After the reaction, PEG–Man SCPs were deprotected by transferring the SCPs in MeOH (5 mL) and reacting with NaOMe (20 eq.) for 30 min followed by washing with methanol. Finally, the synthesized PEG–Man SCPs and PEG–biotin SCPs were washed with water and stored in water with NaN_3 (0.1 wt%).

SCP Characterization: AFM force spectroscopy with a NanoWizard 2 system (JPK instruments AG, Berlin, Germany) was performed to determine the elastic modulus of the microparticles. As AFM probe a glass bead (diameter 4.75 µm) was glued with an epoxy glue onto a tipless, noncoated cantilever (nominal spring constant 0.3 N m^{-1}; CSC12, NanoAndMore GmbH). Several force curves were recorded for all types of SCPs in the respective buffer condition (Man-SCPs in lectin binding buffer, biotin SCPs in PBS, PEG–CA SCPs in aqueous NaCl solutions). Force-indentation data were analyzed with an appropriate contact model developed by Glaubitz et al.[22]

Determination of Functionalization Degree via Toluidine Blue O (TBO) Titration: Carboxylic acid group functionalized SCPs dispersion (0.5 mL) was washed with ethanol and dried under vacuum at 50 °C for 5 h until constant weight was reached. TBO aqueous solution (1 mL, 312.5×10^{-6} M) at pH 10–11 was added to the dry SCPs and shaken in the dark overnight to stain the SCPs. The stained SCP dispersion was centrifuged for 30 min at 4400 rpm. The supernatant (0.3 mL) was diluted with water (1.7 mL). The absorbance at 633 nm of this solution was measured by UV–VIS spectroscopy and compared to the absorbance of a TBO reference solution (312.5×10^{-6} M TBO in aqueous solution at pH 10–11 and 1.7 mL water). The carboxylic group functionalization degree of this group of SCPs was calculated with the following equation $D_{CGF} = N_R(1 - A_S/A_E)/W_{Dry}$, where D_{CGF} is the carboxylic group functionalization degree, A_S and A_R is the UV–VIS absorbance of sample and reference, W_{Dry} is the dry weight of SCP dispersion (0.5 mL), N_R is the amount of TBO in the reference in units of µmol. For each group of SCPs, the TBO titration experiment was repeated three times and the average carboxylic group functionalization degree of the three experiments was used as the carboxylic group functionalization degree of this group of SCPs.

RICM Measurements: Glass slides (15 µ-Slide 8-well, ibidi, Germany) were cleaned in a UV ozone cleaner (UVC-1014, NanoBioAnalytics, Germany) for 30 min. For PEI coated surface, glass slides were immersed in a branched PEI (M_n 10 kDa) water solution (1 m mL^{-1}), shaken for 120 min, flushed with RICM measurement solution. For protein coating, glass slides were immersed in a mixture of ethanol (182.4 mL), water (9.6 mL), acetic acid (192 µL), and GLYMO (glycidoxypropyl trimethoxysilane) (1920 µL), shaken for 120 min, flushed with ethanol, followed by annealing for 120 min at 90 °C. Before RICM measurement, the GLYMO slides were immersed in a Con A or avidin (0.2 mg mL^{-1}, PBS, pH 7.4), shaken for 60 min, and flushed with RICM measurement solution. RICM on an IX 73 inverted microscope (Olympus, Japan) was used to obtain the contact area between the SCPs and the glass coverslip surfaces. For illumination, an Hg-vapor arc lamp was used with a green monochromator (546 nm). An UPlanFL N 60×/0.90 dry objective (Olympus Corporation, Japan) and uEye digtal camera (IDS Imaging Development Systems GmbH, Germany) were used to image the RICM patterns. To conduct the JKR measurements of the adhesion energies, both the contact radius and the particle radius were measured. Images with RICM patterns were read out using self-written image analysis software, contact areas and particle profiles were evaluated using scripted peak finding algorithms (IgorPro Wavemetrics USA).

Supporting Information

Supporting Information is available from the Wiley Online Library or from the author.

Acknowledgements

S.S. acknowledges funding from the German Research Foundation (DFG) within project SCHM 2748/3-1. H.L. acknowledges funding from the DFG within project LO 418/16.

Conflict of Interest

The authors declare no conflict of interest.

Keywords

biointerfaces, biomimetic hydrogels, cell adhesion, glycocalyx, soft colloidal probes

Received: April 18, 2017
Revised: July 6, 2017
Published online:

[1] a) S. Weinbaum, J. M. Tarbell, E. R. Damiano, in *Annual Review of Biomedical Engineering*, Vol. *9*, Annual Reviews, Palo Alto **2007**, p. 121; b) V. Vogel, M. Sheetz, *Nat. Rev. Mol. Cell Biol.* **2006**, *7*, 265; c) E. S. Place, N. D. Evans, M. M. Stevens, *Nat. Mater.* **2009**, *8*, 457.
[2] a) I. Levental, P. C. Georges, P. A. Janmey, *Soft Matter* **2007**, *3*, 299; b) A. J. Engler, S. Sen, H. L. Sweeney, D. E. Discher, *Cell* **2006**, *126*, 677.
[3] a) M. A. Schwartz, D. W. DeSimone, *Curr. Opin. Cell Biol.* **2008**, *20*, 551; b) J. Solon, I. Levental, K. Sengupta, P. C. Georges, P. A. Janmey, *Biophys. J.* **2007**, *93*, 4453.
[4] A. Bershadsky, M. Kozlov, B. Geiger, *Curr. Opin. Cell Biol.* **2006**, *18*, 472.
[5] T. R. Weikl, M. Asfaw, H. Krobath, B. Rozycki, R. Lipowsky, *Soft Matter* **2009**, *5*, 3213.
[6] H. Krobath, B. Rozycki, R. Lipowsky, T. R. Weikl, *Soft Matter* **2009**, *5*, 3354.
[7] M. J. Paszek, D. Boettiger, V. M. Weaver, D. A. Hammer, *PLoS Comput. Biol.* **2009**, *5*, e100604.
[8] L. L. Kiessling, J. C. Grim, *Chem. Soc. Rev.* **2013**, *42*, 4476.

[9] C. Forrey, J. F. Douglas, M. K. Gilson, *Soft Matter* **2012**, *8*, 6385.
[10] C. Jeppesen, J. Y. Wong, T. L. Kuhl, J. N. Israelachvili, N. Mullah, S. Zalipsky, C. M. Marques, *Science* **2001**, *293*, 465.
[11] M. Mammen, S.-K. Choi, G. M. Whitesides, *Angew. Chem. Int. Ed.* **1998**, *37*, 2754.
[12] D. Pussak, M. Behra, S. Schmidt, L. Hartmann, *Soft Matter* **2012**, *8*, 1664.
[13] V. T. Moy, Y. K. Jiao, T. Hillmann, H. Lehmann, T. Sano, *Biophys. J.* **1999**, *76*, 1632.
[14] L. Limozin, K. Sengupta, *ChemPhysChem* **2009**, *10*, 2752.
[15] K. L. Johnson, K. Kendall, A. D. Roberts, *Proc. R. Soc. London, Ser. A* **1971**, *324*, 301.
[16] S. Martin, H. Wang, L. Hartmann, T. Pompe, S. Schmidt, *Phys. Chem. Chem. Phys.* **2015**, *17*, 3014.
[17] S. Schmidt, A. Reinecke, F. Wojcik, D. Pussak, L. Hartmann, M. J. Harrington, *Biomacromolecules* **2014**, *15*, 1644.
[18] D. Pussak, D. Ponader, S. Mosca, S. V. Ruiz, L. Hartmann, S. Schmidt, *Angew. Chem. Int. Ed.* **2013**, *52*, 6084.
[19] S. Martin, H. Wang, T. Rathke, U. Anderegg, S. Möller, M. Schnabelrauch, T. Pompe, S. Schmidt, *Polymer* **2016**, *102*, 342.
[20] D. Pussak, D. Ponader, S. Mosca, T. Pompe, L. Hartmann, S. Schmidt, *Langmuir* **2014**, *30*, 6142.
[21] N. Helfricht, E. Doblhofer, V. Bieber, P. Lommes, V. Sieber, T. Scheibel, G. Papastavrou, *Soft Matter* **2017**, *13*, 578.
[22] M. Glaubitz, N. Medvedev, D. Pussak, L. Hartmann, S. Schmidt, C. A. Helm, M. Delcea, *Soft Matter* **2014**, *10*, 6732.
[23] S. Schmidt, H. Wang, D. Pussak, S. Mosca, L. Hartmann, *Beilstein J. Org. Chem.* **2015**, *11*, 720.
[24] G. Dorman, H. Nakannura, A. Pulsipher, G. D. Prestwich, *Chem. Rev.* **2016**, *116*, 15284.
[25] G. Hild, R. Okasha, M. Macret, Y. Gnanou, *Die Makromol. Chem.* **1986**, *187*, 2271.
[26] P. G. de Gennes, *Scaling Concepts in Polymer Physics*, Cornell University Press, **1979**.
[27] N. M. Green, *Methods Enzymol.* **1990**, *184*, 51.
[28] F. P. Schwarz, K. D. Puri, R. G. Bhat, A. Surolia, *J. Biol. Chem.* **1993**, *268*, 7668.
[29] A. Chen, V. T. Moy, *Biophys. J.* **2000**, *78*, 2814.
[30] A. Chilkoti, P. S. Stayton, *J. Am. Chem. Soc.* **1995**, *117*, 10622.
[31] D. Ponader, F. Wojcik, F. Beceren-Braun, J. Dernedde, L. Hartmann, *Biomacromolecules* **2012**, *13*, 1845.
[32] L. Tao, J. Geng, G. J. Chen, Y. J. Xu, V. Ladmiral, G. Mantovani, D. M. Haddleton, *Chem. Commun.* **2007**, 3441.

